Journal of Directed Energy, **2**, Fall 2006, 107–117

Propagation of High-Energy Laser Beams Through Atmospheric Stagnation Zones

Joseph Peñano,* Phillip Sprangle, and Bahman Hafizi[1]

Plasma Physics Division, Naval Research Laboratory, Washington, D.C. 20375

Stagnation zones, i.e., regions in which the effective transverse wind velocity is zero, can greatly enhance the thermal blooming of high-energy laser beams (HELs) in the atmosphere. An approximate expression for the Strehl ratio of a focused HEL beam propagating through a stagnant zone is derived. The propagation of a HEL beam in a maritime atmosphere is modeled in a fully three-dimensional and time-dependent manner using the HELCAP propagation code. In the simulations, the beam is focused onto a remote target, and a stagnation zone is created by slewing the laser in the direction of the wind. The laser power delivered to the target is calculated as a function of the slew rate. For the parameters considered, it is found that a stagnation zone near the laser source has little effect on the propagation efficiency while a stagnation zone near the target can significantly reduce the power on the target.

KEYWORDS: Atmospheric propagation, High-energy laser, Stagnation zone

1. Introduction

High-energy laser beams (HELs) propagating through the atmosphere can be severely defocused or deflected by thermal blooming.[12] The thermal blooming process is driven by a small fraction of the laser energy that is absorbed by the molecular and aerosol constituents of air.[4,14] The absorbed energy locally heats the air and leads to a decrease in the air density, which modifies the refractive index. The refractive index variation leads to a defocusing or deflection of the laser beam. In the presence of a transverse wind, the region of heated air is convected out of the beam path and a steady-state situation is realized.[12] In general, however, the intensity of a beam undergoing thermal blooming is a function of both time and spatial position, particularly in a stagnation zone, where the effective wind velocity is zero.

Stagnation zones are particularly detrimental to HEL propagation since, without an effective clearing mechanism for the heated air, the strength of the thermal lens grows in time. In this situation, the defocusing process is eventually limited by thermal conduction or buoyancy. However, by the time these processes become effective, the beam may have already been severely degraded.

The importance of stagnation zones for Navy and Air Force applications was recognized in the early 1970s by J.N. Hayes of the Naval Research Laboratory (NRL)[9] and by C. B. Hogge and R. R. Butts of the Air Force Weapons Laboratory.[10] The earliest experiments

Received February 18, 2006; revision received June 15, 2006.

*Corresponding author; e-mail: joseph.penano@nrl.navy.mil.

[1]Icarus Research, Inc., P.O. Box 30780, Bethesda, MD 20824-0780.

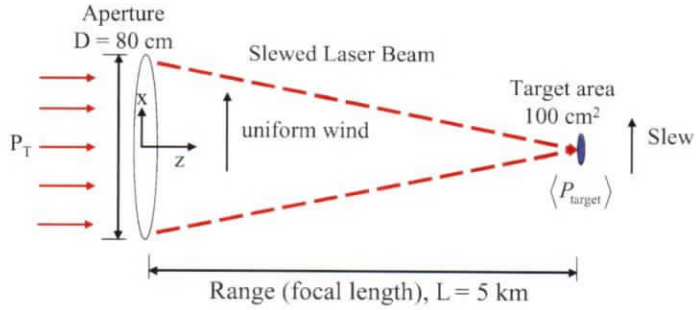

Fig. 1. Schematic diagram showing the simulation geometry. A HEL beam of power P_T is focused at a range of $L = 5$ km in the presence of a uniform wind with speed $V_w = 5$ m/s. The beam is slewed in the direction of the wind to create a stagnation zone along the propagation path.

were performed by P. Berger and F. Gebhardt of United Technologies Research Laboratory.[2] These experiments used a 10-W, CO_2 laser passed through an absorption cell containing CO_2 gas. The cell was pivoted to simulate a wind profile containing a stagnation zone. Time-dependent numerical simulations of these experiments were performed by P. Ulrich and J. Ulrich of NRL.[2] The results of these early experiments and simulations provided basic insights into the effects of stagnation zones on HEL propagation, including the dependence on slew rate and the location of the stagnation zone along the path.

In this study we examine the effect of a stagnation zone on a HEL beam focused onto a remote target in a maritime atmosphere. We first analyze the effect of a stagnation zone on the propagation of a focused beam and calculate an approximate expression for the relative intensity (Strehl ratio) on target as a function of focusing geometry and stagnation zone position. We then utilize the HELCAP code,[14] a three-dimensional, time-dependent numerical simulation, to examine the propagation of a megawatt-class HEL beam through a maritime atmosphere that contains a stationary stagnation zone along the laser path. The laser target configuration used in these simulations is shown in Fig. 1. Our simulation model includes time-dependent thermal blooming as well as aerosol and molecular absorption,[4,14] turbulence,[15] aerosol and molecular scattering,[11] and aerosol heating and vaporization.[1,5,6,17] We use the simulations to calculate the laser power delivered to a remote target for different wind profiles that place the stagnation zone at different locations along the laser propagation path.

2. Analysis of HEL Propagation Through a Stagnation Zone

The effect of a stagnation zone on HEL propagation in the atmosphere is highly dependent on laser and atmospheric parameters as well as on the propagation geometry. In general, the problem requires a numerical simulation to determine the amount of power reaching a remote target. Before presenting results of full-scale propagation simulations, however, it is useful to analyze the following simpler problem.

Consider a focused laser beam of wavelength λ, propagating from $z = 0$ to a remote target at a range $z = L$, where z denotes the propagation coordinate. The focal length of the laser beam L_f is such that $L_f \geq L$. The wind speed $V(z)$ is only a function of z and has a stagnation point defined by $V(z_0) = 0$, where $0 < z_0 < L$. The atmosphere is characterized

by an absorption coefficient α and a scattering coefficient β. Turbulence is neglected in this analysis. This configuration allows an approximate expression for the Strehl ratio (relative intensity) at the target to be calculated analytically as a function of both the location of the absorbing region and the laser focal length.

The propagation of the laser beam is described by the paraxial wave equation

$$\frac{\partial A}{\partial z} = \left(\frac{i}{2k_0}\nabla_\perp^2 + i\frac{\omega_0}{c}\delta n_{\mathrm{TB}} - \frac{\beta}{2}\right)A, \tag{1}$$

where the laser electric field is $\boldsymbol{E} = A\exp[i(\omega_0 z/c - \omega_0 t)]\hat{\boldsymbol{e}}_x/2 + \text{c.c.}$, $\omega_0 = 2\pi c/\lambda$, $\hat{\boldsymbol{e}}_x$ is a unit polarization vector in the x direction, $k_0 = n_0\omega_0/c$, n_0 is the ambient refractive index, $\nabla_\perp$ is the gradient operator in the transverse direction, c is the speed of light in vacuum, δn_{TB} is the change in refractive index induced by the laser, and c.c. denotes the complex conjugate. In the absence of a transverse wind or slew, there is axial symmetry about the z axis and all spatially varying quantities are functions of (r, z, t) only, where r is the radial coordinate and t is time. Writing $A(r, z, t) = B(r, z, t)\exp[i\theta(r, z, t)]$, where B, θ, and δn_{TB} are assumed to be real, leads to the following equations for the laser intensity $I(\sim B^2)$ and the transverse wave number $\boldsymbol{k}_\perp = \nabla_\perp\theta$:

$$\frac{\partial I}{\partial z} = -\frac{1}{k_0}\nabla_\perp\cdot(\boldsymbol{k}_\perp I) - \beta I, \tag{2}$$

$$\frac{\partial \boldsymbol{k}_\perp}{\partial z} = \frac{1}{8k_0}\nabla_\perp\left\{\frac{1}{I^2}\left[2I\nabla_\perp^2 I - (\nabla_\perp I)^2\right]\right\} - \frac{1}{k_0}\boldsymbol{k}_\perp\cdot\nabla_-\boldsymbol{k}_\perp + \frac{\omega_0}{c}\nabla_\perp\delta n_{\mathrm{TB}}. \tag{3}$$

On the right-hand side of Eq. (3), the first term is of order $\sim\lambda/R^3$, where R is the laser spot size. The second term is of order $\sim R/(L_f^2\lambda)$ for a focused beam, and the third term is of order $\sim\delta n_{\mathrm{TB}}/(\lambda R)$. We consider parameters such that $R\sim 50$ cm, $\lambda\sim 1$ μm, and $L_f\sim 5$ km. In this parameter regime, the second term is much larger than the first term. The third term is much larger than the second term for $\delta n_{\mathrm{TB}} > 10^{-8}$, which is typically encountered within a stagnation zone. Hence, for the parameter regime of interest, we neglect the first and second terms on the right-hand side of Eq. (3) and integrate to solve for $\boldsymbol{k}_\perp$, i.e.,

$$\boldsymbol{k}_\perp(r, z, t) \approx \boldsymbol{k}_{\perp 0}(r) + \frac{\omega_0}{c}\int_0^z \nabla_\perp\delta n_{\mathrm{TB}}(r, z', t)\,dz', \tag{4}$$

where $\boldsymbol{k}_{\perp 0}(r)$ is the initial transverse wave number at $z = 0$. Equation (4) represents $\boldsymbol{k}_\perp$ in the geometric optics limit.

Equation (2) can be integrated to yield

$$I(r, z, t) = I(r, 0, t)e^{-\beta z}\exp\left\{-\frac{c}{\omega_0}\int_0^z \frac{1}{I(r, z', t)}\nabla_\perp\cdot[\boldsymbol{k}_\perp(r, z', t)I(r, z', t)]dz'\right\}, \tag{5}$$

which is an integral equation for $I(r, z, t)$ that can be solved approximately by replacing $I(r, z, t)$ on the right-hand side by $I_0(r, z)$, i.e., the unperturbed intensity for a homogeneous medium ($\delta n_{\mathrm{TB}} = 0$). The unperturbed intensity satisfies

$$I_0(r, z) = I(r, 0)e^{-\beta z}\exp\left\{-\frac{c}{\omega_0}\int_0^z \frac{1}{I_0(r, z')}\nabla_\perp\cdot[\boldsymbol{k}_{\perp 0}(r)\,I_0(r, z')]\,dz'\right\}. \tag{6}$$

Substituting Eq. (4) into Eq. (5) yields the relative intensity[8]

$$\frac{I(r, z, t)}{I_0(r, z)} = \exp\left\{-\int_0^z \frac{dz'}{I_0(r, z')}\nabla_\perp\cdot\left[I_0(r, z')\int_0^{z'} dz''\nabla_\perp\delta n_{\mathrm{TB}}(r, z'', t)\right]\right\}. \tag{7}$$

The refractive index change due to thermal blooming is given by $\delta n_{\rm TB} = (n_0 - 1)\delta\rho/\rho_0$, where ρ_0 is the mass density and $\delta\rho$ is the perturbed mass density. In the isobaric regime, the mass density change is given by[12,14]

$$C_p T_0 \left(\frac{\partial}{\partial t} + \boldsymbol{V} \cdot \nabla - \frac{\kappa}{C_p \rho_0} \nabla^2 \right) \delta\rho = -\alpha_{\rm TB}(\boldsymbol{r}, t) I, \tag{8}$$

where κ is the thermal conductivity, $\boldsymbol{V}$ is the effective wind velocity, C_p is the specific heat at constant pressure, T_0 is the ambient temperature, and I is the time-averaged laser intensity. In general, the absorption coefficient $\alpha_{\rm TB}$ contains both aerosol and molecular contributions and can be time dependent. For the simplified analysis of this section, however, we take it to be constant in time. The isobaric approximation is valid for times greater than the hydrodynamic time R/C_s, where C_s is the acoustic speed. We consider time scales less than the thermal conduction time, $C_p \rho_0 R^2/\kappa$, and neglect the thermal conduction term in Eq. (8).

For the purpose of obtaining an approximate closed-form expression for Eq. (7), we solve Eq. (8) approximately by writing the operator $\boldsymbol{V} \cdot \nabla \approx 1/\tau_c(z)$, where $\tau_c(z) = R(z)/|V(z)|$ is the clearing time. Using this approximation, we can integrate Eq. (8) to obtain

$$\delta n_{\rm TB}(r, z, t) \approx -\gamma_{\rm TB} \alpha I_0(r, z) \tau_c(z) \{1 - \exp[-t/\tau_c(z)]\}, \tag{9}$$

where $\gamma_{\rm TB} \equiv (n_0 - 1)/(C_p T_0 \rho_0)$.

The unperturbed intensity is taken to have a Gaussian transverse profile:

$$I_0(r, z) = \frac{I_{00} R_0^2}{R^2(z)} \exp\left[-\frac{r^2}{R^2(z)} \right] e^{-\beta z}, \tag{10}$$

where I_{00} denotes the intensity on axis at $z = 0$. The spot size R is a function of z, and the initial spot size is denoted by $R_0 \equiv R(z = 0)$. Substituting Eqs. (9) and (10) into Eq. (7) results in an expression for the on-axis Strehl ratio at $z = L$, i.e.,

$$\frac{I(r = 0, L, t)}{I_0(r = 0, L)} = \exp\left[-8 I_{00} R_0^2 \gamma_{\rm TB} \alpha \int_0^L dz' \int_0^{z'} dz'' G(z'', t) \right], \tag{11}$$

where $G(z, t) = \tau_c(z)\{1 - \exp[-t/\tau_c(z)]\} \exp(-\beta z)/R^4(z)$. To obtain an approximate analytic expression for the right-hand side of Eq. (11), we note that for a weakly focused beam, the integrand G is sharply peaked and grows linearly with time in the vicinity of the stagnation zone, i.e., $G(z_0, t) = t \exp(-\beta z_0)/R^4(z_0)$. Hence, we can approximate the integration over z'' in Eq. (11) by

$$\int_0^{z'} dz'' G(z'', t) \approx G(z_0, t) \Delta z \Theta(z' - z_0), \tag{12}$$

where Δz is the characteristic width of the stagnation region and Θ is the Heaviside step function.

Using Eq. (12) in Eq. (11) results in

$$\frac{I(r = 0, L, t)}{I_0(r = 0, L)} \approx \exp\left[-\frac{8 \gamma_{\rm TB} \alpha I_{00} L^2 t}{R_0^2} \left(\frac{\Delta z}{L} \right) \left(1 - \frac{z_0}{L} \right) \frac{R_0^4 \exp(-\beta z_0)}{R^4(z_0)} \right]. \tag{13}$$

The width of the stagnation region Δz is in general a function of time and also the spatial variation of the wind profile. We can define the stagnation zone as the region where the condition $t/\tau_c(z) \ll 1$ is satisfied. In this case, the width of the stagnation zone can be defined according to $t/\tau_c(z_0 + \Delta z) = 1$.

We now consider specific analytic expressions for the wind profile $V(z)$ and laser spot size $R(z)$. For a slewed laser beam, the wind profile can be written as

$$V(z) = V_{\text{wind}}(1 - z/z_0), \tag{14}$$

where V_{wind} is the ambient wind velocity and the laser slew rate $\dot{\theta}$ is related to z_0 according to $\dot{\theta} = V_{\text{wind}}/z_0$. Note that for this model, a stagnation zone at the transmitter ($z = 0$) implies an infinite slew rate. Assuming that the laser spot size does not vary appreciably within the stagnation zone,

$$\Delta z \approx z_0 R(z_0)/(V_{\text{wind}} t) \tag{15}$$

for the wind profile of Eq. (14).

For the linearly varying wind profile described above, Eq. (13) can be written as

$$\frac{I(r = 0, L, t)}{I_0(r = 0, L)} \approx \exp\left[-\frac{8\gamma_{\text{TB}}\alpha I_{00} L^2}{R_0 V_{\text{wind}}} f(z_0)\right], \tag{16}$$

where

$$f(z_0) = \left(\frac{z_0}{L}\right)\left(1 - \frac{z_0}{L}\right)\frac{R_0^3 \exp(-\beta z_0)}{R^3(z_0)} \tag{17}$$

describes how the location of the stagnation zone affects the relative intensity on target. The larger the value of $f(z_0)$, the lower the intensity on the target.

We can derive an approximate functional form for $R(z)$ to be used in Eq. (17). Substituting Eq. (10) into Eq. (6), the laser spot size can be shown to satisfy $R(z) = R_0[1 - z(1 - \eta)/L]$ for $z \ll L_f$, where the parameter $\eta \equiv R(L)/R_0$, i.e., the ratio of the spot size on target to the initial spot size. In terms of the focal length, $\eta = 1 - (L/L_f)$. Phenomenologically, η can also parameterize focusing limitations due to beam quality or atmospheric turbulence.

Figure 2 plots the distortion function f versus z_0 for various values of η. We assume a normalized scattering coefficient of $\beta L = 0.25$. For a beam that is focused near the target plane, the distortion at the target plane is largest when the stagnation zone is close to the target. In contrast, when the beam is collimated ($\eta \sim 1$), the distortion at the target plane is greater when the stagnation zone is closer to the laser source. Note that the case $z_0 = 0$,

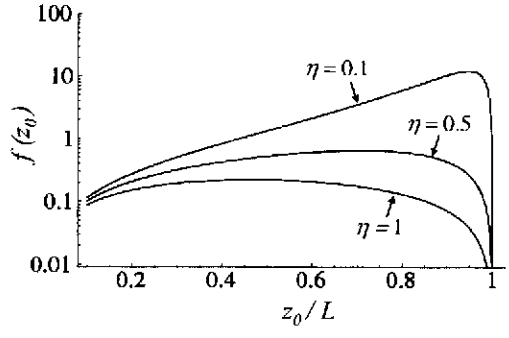

Fig. 2. Distortion function f as defined by Eq. (17) plotted versus distance to stagnation zone z_0 for various values of the focusing parameter $\eta = R(L)/R_0$, where $R(L)$ is the unperturbed laser spot size at the target plane ($z = L$), R_0 is the initial spot size at $z = 0$, and $\beta L = 0.25$.

which corresponds to an infinite slew rate given the assumed wind profile of our model, is not physically realizable.

3. Numerical Simulation

The propagation code used in this study is HELCAP (High Energy Laser Code for Atmospheric Propagation), which is a fully time-dependent, three-dimensional code developed at the NRL. HELCAP models the propagation of continuous and pulsed HELs through various atmospheric environments. It includes the effects of aerosol and molecular scattering, aerosol heating and vaporization, thermal blooming due to both aerosol and molecular absorption, and atmospheric turbulence. A more detailed description of the code can be found in Refs. 13 and 14.

HELCAP solves a nonlinear Schrödinger-like equation for the complex laser electric envelope, $A(x, y, z, t)$, which is of the form

$$\frac{\partial A}{\partial z} = \frac{ic}{2\omega_0}\nabla_\perp^2 A + \left[i\frac{\omega_0}{c}(\delta n_T + \delta n_{TB}) - \frac{1}{2}(\alpha_{TB} + \beta)\right]A + \sum_j S_j, \tag{18}$$

where $A(x, y, z, t)$ is the complex laser electric field amplitude and the terms denoted by $\sum_j S_j$ represent other physical processes that are included in the code but are not important for the parameter regime considered here. The laser intensity is $I = cAA^*/8\pi$. The absorption and scattering coefficients α_{TB} and β, respectively, contain both molecular and aerosol contributions. In general, they are time dependent due to aerosol heating and vaporization by the laser as described in Ref. 14. The quantities δn_T and δn_{TB} denote the refractive index variation due to atmospheric turbulence and thermal blooming, respectively. Atmospheric turbulence is modeled in the usual manner using phase screens for which the scale sizes of the index fluctuations are described by a Kolmogorov spectrum characterized by the parameter C_n^2 (Ref. 15). The mass density change due to thermal blooming is solved according to Eq. (8), where the total absorption coefficient α_{TB} is time dependent and contains both aerosol and molecular contributions in the manner described in Ref. 14.

For the numerical simulations presented here, we consider a slewed HEL focused at a range of $L = 5$ km in the presence of a uniform transverse wind. The z axis defines the direction of propagation, and the wind and slew velocities are taken to be along the y axis. The simulation geometry is shown in Fig. 1. The HEL has an initial field profile given by $A = A_0 f(r) g(t) \exp(-r^2/R_0^2)$, where $f(r) = \exp[-(2r/D)^\ell]$, $\ell = 20$, limits the transverse extent of the beam to the aperture diameter D. The function $g(t)$ is the initial temporal profile of the beam, which contains a pointing jitter characterized by an angular spread of 2 μrad and a white noise temporal spectrum. The transmitted power at the source is denoted by P_T.

The laser is propagated through a maritime environment in which the aerosol distribution is modeled using the Advanced Navy Aerosol Model (ANAM),[16] and the molecular absorption coefficient is calculated using MODTRAN4.[3] The details of the atmospheric model and the parameters used to characterize a maritime environment are discussed in Ref. 14. The atmospheric parameters used in these simulations are identical to the maritime propagation simulations of Ref. 14, which are characteristic of a moderately stressing maritime environment.[7] The ambient absorption and scattering coefficients for propagation at $\lambda = 2.141$ μm are $\alpha_{TB} = 6 \times 10^{-3}$ km^{-1} and $\beta = 0.05$ km^{-1}, respectively. In the simulations these quantities vary in space and time due to aerosol vaporization.

The effective wind speed along the propagation path is $V(z) = V_{\text{wind}} - \dot{\theta} z$, where z is the distance from the laser source, V_{wind} is the ambient wind speed, and $\dot{\theta}$ is the laser beam slew rate. For positive $\dot{\theta}$, i.e., slewing in the direction of the wind, a stagnation zone is created at location $z_0 = V_{\text{wind}}/\dot{\theta}$. In what follows, we investigate the effect of this stagnation zone on the propagation of a HEL for various slew rates, which change the distance between the transmitter and the stagnation zone.

4. Results

We consider a laser of wavelength $\lambda = 2.141$ μm and power $P_T = 1.5$ MW propagating through a maritime atmosphere with $V_{\text{wind}} = 5$ m/s. The power delivered to a target of circular area 100 cm^2 at a range of 5 km is used as a figure of merit. In the simulations that follow, the target is always located such that the peak laser fluence at a 5-km range is at the center of the target. The average power reaching the target is defined by

$$\langle P_{\text{target}} \rangle = \frac{1}{\tau_{\text{dwell}}} \int_0^{\tau_{\text{dwell}}} \mathrm{d}\tau \int \mathrm{d}x\mathrm{d}y I(x, y, z = L, \tau), \tag{19}$$

where the dwell time $\tau_{\text{dwell}} = 1$ s and $\mathrm{d}x\mathrm{d}y$ is the differential cross section, which is integrated over the target area. The total laser energy reaching the target is $E_{\text{target}} = \langle P_{\text{target}} \rangle \tau_{\text{dwell}}$.

Figure 3 plots $\langle P_{\text{target}} \rangle$ versus slew rate $\dot{\theta}$ for the propagation configuration of Fig. 1. A negative slew denotes that the slew direction is opposite to the wind direction. In this case, there is no stagnation zone between the laser and the target. A positive slew denotes slew in the direction of the wind. In this case, it is possible to have a stagnation zone somewhere along the propagation path. For example, a slew rate of 1 mrad/s places the stagnation zone at the target, while a slew rate of 5 mrad/s places the stagnation zone 1 km from the laser source. Figure 3 shows that in the absence of slew (i.e., uniform wind), the power on target is $\langle P_{\text{target}} \rangle \approx 0.7$ MW and the propagation efficiency is ~50%. $\langle P_{\text{target}} \rangle$ increases relative to this value when the slew is opposite to the wind direction because the effectively larger wind speed along the entire propagation path mitigates thermal blooming. For a slew rate $\dot{\theta} = -5$ mrad/s, for example, $\langle P_{\text{target}} \rangle \approx 1.1$ MW, which corresponds to a propagation efficiency of >70%.

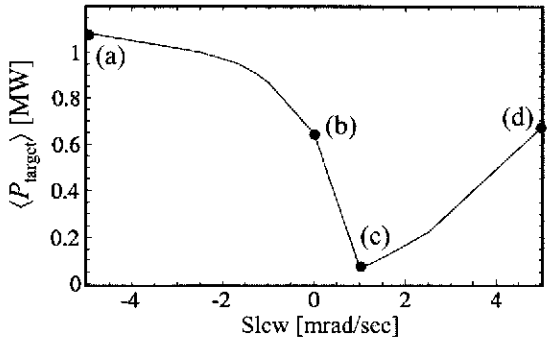

Fig. 3. Average power on target $\langle P_{\text{target}} \rangle$ versus slew rate for $\lambda = 2.141$ μm, $P_T = 1.5$ MW, $V_{\text{wind}} = 5$ m/s, $\tau_{\text{dwell}} = 1$ s, and $L = 5$ km. Points (a), (b), (c), and (d) are labeled to correspond with fluence distributions shown in Fig. 4.

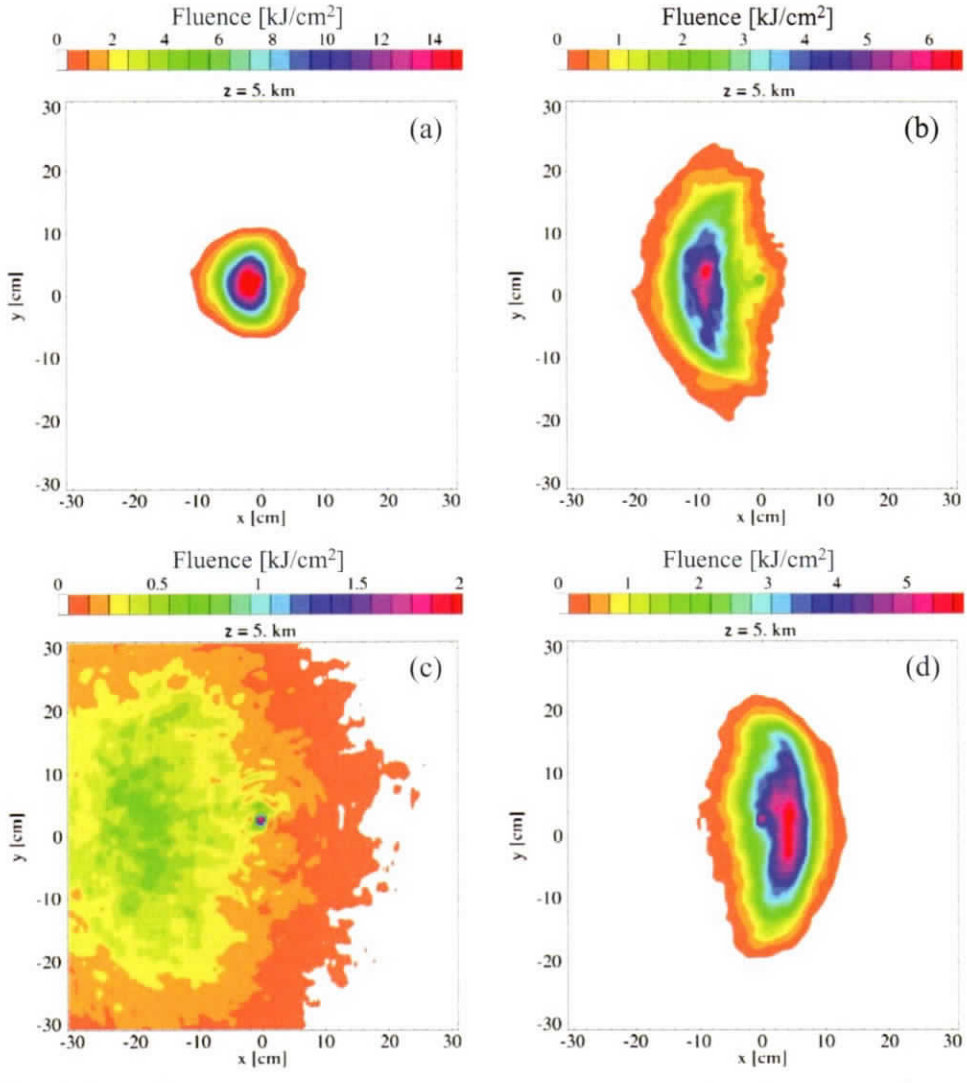

Fig. 4. Laser fluence profiles at the target range for slew rates (a) $\dot{\theta} = -5$ mrad/s, (b) $\dot{\theta} = 0$, (c) $\dot{\theta} = 1$ mrad/s, and (d) $\dot{\theta} = 5$ mrad/s. Parameters are the same as those of Fig. 2. Fluence is calculated over a 1-s dwell time.

When the slew is increased in the direction of the wind, the power on target decreases sharply for $\dot{\theta} < 1$ mrad/s and reaches a minimum when $\dot{\theta} = 1$ mrad/s, i.e., when the stagnation zone is at the target. At this minimum, $\langle P_{\text{target}} \rangle \approx 0.07$ MW, which corresponds to a propagation efficiency of <5%. Increasing the slew rate further brings the stagnation zone closer to the laser source, where the intensity is lower, and increases the effective wind velocity near the target. The result is that the power on target increases with slew rate. For a slew rate of $\dot{\theta} = 5$ mrad/s, $\langle P_{\text{target}} \rangle \approx 0.7$ MW. These results are consistent with the calculation in Sec. 2, i.e., for a beam focused onto the target plane, a stagnation zone close to the target will result in the largest beam distortion.

Figure 4 plots the laser fluence on target calculated over a 1-s dwell time. Panel labels a, b, c, and d correspond to the different slew rates indicated in Fig. 3. Panel a corresponds to a slew rate $\dot{\theta} = -5$ mrad/s, which gives the maximum power on target over the range of slew rates considered. The beam is well focused and exhibits practically no thermal blooming effects. Panel b shows the beam profile when the slew rate is zero, i.e., a uniform wind profile. In this case the beam fluence profile shows the characteristic crescent shape associated with thermal blooming with the centroid of the beam deflected opposite to the direction of the wind. Panel c shows the beam profile on target for the case when the stagnation zone is at the target. The beam is severely defocused as a result of thermal blooming. The peak in fluence near ($x = 0$, $y = 0$) is due to the leading edge of the beam ($t < 20$ ms), which is not affected by the time-dependent thermal blooming process. Panel d shows the beam profile when the stagnation zone is 1 km from the target. In this case, the effective wind velocity near the target is in the opposite direction relative to that of panel b. The value of $\langle P_{\text{target}} \rangle$ is similar to that of panel b but with the beam deflected in the opposite direction.

Figure 5 shows the time dependence of the beam intensity at the target. Figure 5a corresponds to a slew rate of $\dot{\theta} = -5$ mrad/s, when the power on target is maximum. In this case the beam is well focused over the entire dwell time. The transverse profile is mainly affected by turbulence and pointing jitter. Figure 5b corresponds to a slew rate of $\dot{\theta} = 1$ mrad/s, which results in the minimum power on target. For this case, it is seen that severe defocusing occurs

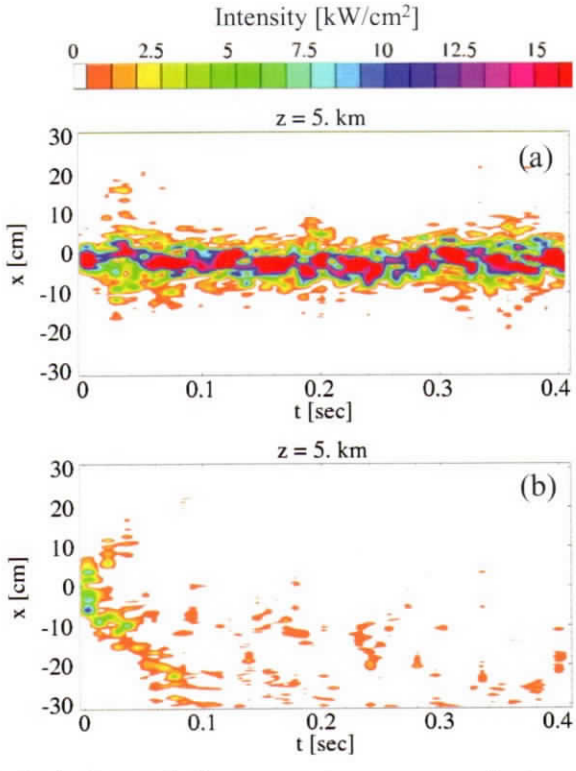

Fig. 5. Laser intensity in the $y = 0$ plane versus transverse coordinate x and time t for slew rates (a) $\dot{\theta} = -5$ mrad/s and (b) $\dot{\theta} = 1$ mrad/s. Parameters correspond to those of Fig. 2.

for times >20 ms, while the first ~10 ms of the beam is relatively unaffected by thermal blooming.

In situations in which the beam director and a rapidly moving target are at different heights, the vertical slew of the HEL may partially mitigate the effect of a stagnation zone near the target. Consider a situation in which the target is a missile at a range of 5 km and an altitude of 5 m, with an incoming velocity of 300 m/s. The beam director is at an altitude of 20 m. In this case, the vertical slew rate is ~0.2 mrad/s and the effective vertical wind velocity near the target is ~0.9 m/s. However, from Fig. 3, it can be inferred that the additional slew of ~0.2 mrad/s would have a minor effect on the power on target, including a situation in which the stagnation zone is near the target.

5. Conclusions

Stagnation zones can significantly degrade the propagation efficiency of a high-energy laser beam (HEL) through the atmosphere. We have analyzed the propagation of a focused HEL through a model atmosphere containing a stagnation zone. Our analysis shows that the amount of laser degradation caused by a stagnation zone is highly dependent on the focusing geometry of the laser beam and the location of the stagnation zone along the propagation path. For a collimated laser beam, a stagnation zone near the transmitter causes the largest distortion of the laser beam on the target. For a laser that is focused onto the target, a stagnation zone near the target causes the largest laser distortion and the fastest decrease in laser intensity. This finding is in agreement with the experimental results of Ref. 2.

We use a full-scale numerical simulation (HELCAP) to model the propagation of a megawatt-class HEL through a realistic maritime atmosphere containing a stationary stagnation zone. The HEL is focused onto a remote target. The stagnation zone is created by slewing the HEL in the direction of the wind, and the location of the stagnation zone is varied by changing the slew rate. Consistent with our analysis, the simulations show that the power on target is minimized when the slew rate is such that the stagnation zone is located near the target plane. In this case, propagation efficiency can be reduced by an order of magnitude relative to an unslewed beam.

6. Acknowledgments

This work was sponsored by the Joint Technology Office and the Office of Naval Research.

References

[1]Armstrong, R.L., Appl. Opt. **23**, 148 (1984); Armstrong, R.L., J. Appl. Phys. **56**, 2142 (1984); Armstrong, R.L., S.A.W. Gerstl, and A. Zardecki, J. Opt. Soc. Am. A **2**, 1739 (1985).

[2]Berger, P.J., P.B. Ulrich, J.T. Ulrich, and F.G. Gebhardt, Appl. Opt. **16**, 345 (1977).

[3]Berk, A., G.P. Anderson, P.K. Acharya, J.H. Chetwynd, L.S. Bernstein, E.P. Shettle, M.W. Matthew, and S.M. Adler-Golden, "MODTRAN4 User's Manual" (1999).

[4]Brown, R.T., and D.C. Smith, J. Appl. Phys. **46**, 402 (1975).

[5]Caledonia, G.E., and J.D. Teare, J. Heat Transfer **99**, 281 (1977).

[6]Davies, S.C., and J.R. Brock, App. Opt. **26**, 786 (1987).

[7]Doss-Hammel, S., D. Tsintikidis, D. Merritt, and J. Fontana, Proc. SPIE **5552**, 208 (2004).

[8]Gebhardt, F.G., and D.C. Smith, IEEE J. Quant. Elec. **7**, 63 (1971); Buser, R.G., R.S. Rohde, P.J. Berger, F.G. Gebhardt, and D.C. Smith, Appl. Opt. **14**, 2740 (1975).

[9]Hayes, J.N., Technical Report NRL-FR-7213, Naval Research Laboratory, Washington, DC (1971).

[10]Hogge, C.B., and R.R. Butts, Technical Report AFWL-TR-73-76, Air Force Weapons Laboratory, Kirkland Air Force Base, NM (1973).

[11]Measures, R.M., *Laser Remote Sensing, Fundamentals and Applications*, Krieger, Malabar, FL (1992).

[12]Smith, D.C., Proc. IEEE **65**, 1679 (1977).

[13]Sprangle, P., J.R. Peñano, and B. Hafizi, Phys. Rev. E **66**, 046418 (2002); Peñano, J.R., P. Sprangle, B. Hafizi, A. Ting, D.F. Gordon, and C.A. Kapetanakos, Phys. Plasmas **11**, 2865 (2004).

[14]Spangle, P., J.R. Peñano, and B. Hafizi, "Optimum Wavelength and Power for Efficient Laser Propagation in Various Atmospheric Environments," NRL/MR/6790-05-8907 (2005).

[15]*The Infrared and Electro-Optical Systems Handbook*, vol. 2, edited by F.G. Smith, Environmental Research Institute of Michigan, Ann Arbor, MI, and SPIE Optical Engineering Press, Bellingham, WA (1993).

[16]van Eijk, A.M.J., and L.H. Cohen, "The ANAM-3.0 Development," TNO Physics and Electronics Laboratory, June 2005; Piazzola, J., M.J. van Eijk, and G. de Leeuw, Opt. Eng. **39**, 1620 (2000); Zeisse, C.R., "NAM6: Batch Code for the Navy Aerosol Model," Technical Report 1804, SPAWAR Systems Center, San Diego, CA, Oct. 1999.

[17]Williams, F.A., Int. J. Heat Mass Transfer **8**, 575 (1965).

The Authors

Dr. Bahman Hafizi received B.Sc. and Ph.D. degrees in physics from Imperial College, London, in 1974 and 1978. He is president of Icarus Research, Inc. He was previously a Research Associate in the Department of Astro-Geophysics at the University of Colorado and a Staff Scientist for SAIC. His research areas include propagation of ultraintense laser pulses, laser-driven electron accelerators, laser–plasma interactions, nonlinear optics, advanced sources of electromagnetic radiation with application to imaging, lithography, and remote sensing. He is an Associate of the Royal College of Science and a member of the American Physical Society, the European Physical Society, and the IEEE.

Dr. Joseph R. Peñano received B.S. and Ph.D. degrees in plasma physics from the University of California, Los Angeles, in 1991 and 1998. He joined the NRL Beam Physics Branch in 2001. He conducts research on atmospheric propagation of ultrashort, high-intensity laser pulses for directed energy weapons and electronic countermeasure applications, advanced radiation sources, and laser-driven particle accelerators. He is the chief developer of HELCAP (High Energy Laser Code for Atmospheric Propagation). Prior to joining NRL, he held a National Research Council postdoctoral fellowship. He received the NRL Alan Berman Publication Award in 2003.

Dr. Phillip Sprangle received his Ph.D. in applied physics from Cornell University in 1973. He is Chief Scientist and Head of the Beam Physics Branch at NRL. His research areas include atmospheric laser propagation, free-electron lasers, and laser acceleration physics. Dr. Sprangle is a fellow of the American Physical Society, the IEEE, and the DEPS. He won the International Free Electron Laser Prize (1991), E.O. Hulburt Science and Engineering Award (1986), and Sigma Xi Pure Science Award (1994), as well as numerous publication awards. He has published more that 200 refereed scientific articles (28 letters) and holds 12 U.S. invention patents.